How to cite: *Angew. Chem. Int. Ed.* **2024**, *63*, e202316786
doi.org/10.1002/anie.202316786

Li–S Batteries

Partially Ion-Paired Solvation Structure Design for Lithium-Sulfur Batteries under Extreme Operating Conditions

Guorui Cai[+], Hongpeng Gao[+], Mingqian Li[+], Varun Gupta, John Holoubek, Tod A. Pascal, Ping Liu, and Zheng Chen**

Abstract: Achieving increased energy density under extreme operating conditions remains a major challenge in rechargeable batteries. Herein, we demonstrate an all-fluorinated ester-based electrolyte comprising partially fluorinated carboxylate and carbonate esters. This electrolyte exhibits temperature-resilient physicochemical properties and moderate ion-paired solvation, leading to a half solvent-separated and half contact-ion pair in a sole electrolyte. As a result, facile desolvation and preferential reduction of anions/fluorinated co-solvents for LiF-dominated interphases are achieved without compromising ionic conductivity ($>1\ mS\,cm^{-1}$ even at $-40\,°C$). These advantageous features were found to apply to both lithium metal and sulfur-based electrodes even under extreme operating conditions, allowing stable cycling of Li||sulfurized polyacrylonitrile (SPAN) full cells with high SPAN loading ($>3.5\ mAh\,cm^{-2}$) and thin Li anode (50 μm) at −40, 23 and 50 °C. This work offers a promising path for designing temperature-resilient electrolytes to support high energy density Li metal batteries operating in extreme conditions.

Introduction

Lithium-sulfur (Li-S) batteries have garnered significant attention in energy storage, attributed to their impressive theoretical energy density of $2600\ Wh\,kg^{-1}$ and the abundant availability of low-cost sulfur.[1] However, the insulating nature of sulfur and solid discharged products of Li_2S_2/Li_2S makes them electrochemically inert, thereby posing substantial challenges in realizing the full potential of Li-S battery technology. The shuttle effect caused by soluble polysulfide intermediates further complicates the electrochemical performance of these batteries.[2] The aforementioned issues would be further aggravated under extreme operating conditions. To address these issues, researchers have turned their attention to sulfur composites, with a specific focus on sulfurized polyacrylonitrile (SPAN).[2c,3] By leveraging the covalent bond between polyacrylonitrile and short-chain sulfur within the conductive SPAN host, a solid-to-solid conversion mechanism is enabled during the charging and discharging processes of the SPAN without the need for soluble polysulfides. The exceptional conductivity and absence of polysulfide formation of this composite material offer promising prospects for overcoming the limitations associated with sulfur electrodes in Li-S batteries.

In addition to the cathode materials, the electrolyte chemistry also plays a crucial role in the Li-S battery performances, especially in extreme conditions. The widely used ether-based electrolytes in Li-S batteries, including dimethoxyethane (DME), 1,3-dioxolane (DOL), and other large-sized multi-glyme solvents, are generally stable against the Li metal anode and polysulfide intermediates but not adaptable for the SPAN.[4] The high solubility of glyme-based solvents induces the polysulfide dissolution from the SPAN, leading to capacity fading. Although increasing salt concentration can alleviate the shuttling effects, the increased viscosity renders sluggish kinetics and significant capacity decay, especially at subzero temperature conditions.[5] Recent works showed that typical ether-based electrolytes (e.g., DOL/DME system) encountered dendritic Li metal growth at subzero temperatures, probably due to the increased charge-transfer resistance at subzero temperatures.[6] Our previous work showed that monodentate ether (e.g., diethyl ether) can partially address this limitation by providing facile desolvation kinetics.[7] Although it has been shown as an effective solvent for ultralow temperatures, it is not stable at elevated temperatures.[8] Its high volatility raises safety concerns due to its high flammability. The local high-concentration

[*] Dr. G. Cai,[+] H. Gao,[+] J. Holoubek, Prof. T. A. Pascal, Prof. P. Liu, Prof. Z. Chen
Department of NanoEngineering,
University of California, San Diego
La Jolla, CA 92093 (USA)
E-mail: jholoube@eng.ucsd.edu
zhengchen@eng.ucsd.edu

M. Li,[+] V. Gupta, Prof. T. A. Pascal, Prof. P. Liu, Prof. Z. Chen
Program of Materials Science and Engineering,
University of California, San Diego
La Jolla, CA 92093 (USA)

Prof. T. A. Pascal, Prof. P. Liu, Prof. Z. Chen
Sustainable Power and Energy Center,
University of California, San Diego
La Jolla, CA 92093 (USA)

Prof. T. A. Pascal, Prof. P. Liu, Prof. Z. Chen
Program of Chemical Engineering,
University of California, San Diego
La Jolla, CA 92093 (USA)

[+] These authors contributed equally to this work.

electrolytes (LHCEs) by using a highly fluorinated diluent as a nonflammable antisolvent in the high concentration of monodentate ether-based electrolytes could simultaneously provide the Li metal anode with improved reversibility at a wide-temperature condition and also reduce the flammability of the whole electrolytes.[6b] Despite the high Li metal Coulombic efficiency (CEs), recent works indicated that practical cells (SPAN loading $>3\,mAh\,cm^{-2}$) with ether-based LHCEs typically fail to achieve stable long-term cycling due to soft-shorting events related to poor ion transport.[9] The reduced ionic conductivity has been found to be a character for heavily ion-paired electrolytes, e.g., LHCEs, and electrolytes with weak solvating solvents including highly fluorinated solvents and monodentate ethers.[9b,10]

To ensure the stability of redox-active sulfur species covalently bonded in the conductive SPAN host, ester-based electrolytes are generally employed, due to the low solubility toward polysulfides.[2c,3] The high melting point of carbonate electrolytes limits the application of Li||SPAN batteries at low temperatures.[11] Carboxylate esters with low melting points and viscosity are commonly employed to improve low-temperance performance.[12] Nevertheless, these molecules display high reactivity with the Li metal, resulting in reduced cycling performance and even hazardous dendrite growth, especially at extreme temperatures. To enhance the compatibility of Li metal with carboxylate ester-containing electrolytes, prior studies explored fluorinated additives to promote the formation of LiF-rich solid electrolyte interphase (SEI) on the anode aiming to improve cycling performance at ambient conditions. Unfortunately, these merits fail to sustain at ultralow temperatures ($<-30\,°C$).[5a,12a,13] Achieving stable cycling of high areal loading of Li-S batteries under both extreme temperatures poses a significant challenge because the electrolytes employed in such batteries need to meet multiple criteria simultaneously, including decent ionic conductivity, low flammability, and excellent compatibility with both lithium metal anodes and sulfur-based cathodes across a wide range of operating temperatures.

Both soft and strong solvents have been used to construct different solvation electrolytes. The soft solvents with weak Li^+ binding have proven to be essential for achieving favorable temperature-dependent Li metal reversibility.[7–8] This is attributed to their ability to facilitate desolvation and form an ion-pairing solvation. The electrolyte featuring contact-ion pair (CIP) structure ensures a preferential reduction of anions, forming a ceramic-dominated SEI. This SEI fosters a high interfacial energy that effectively suppresses the growth of Li dendrites and maintains a low charge transfer impedance.[14] However, such weakly solvating electrolytes commonly lead to the formation of aggerated ion clusters, causing sluggish ion migration.[9b,10] Consequently, prior studies have primarily been adaptable to low energy density cells, despite achieving apparent performance improvement at subzero temperatures.[12] Conversely, solvents with strong solvating capabilities allow for fully solvent-separated ion pair (SSIP) structure, facilitating ion migration. However, they tend to induce a sluggish desolvation and organic-rich SEI derived from the preferential reduction of solvents. This results in high charge transfer impedance and a strong interaction with Li, promoting the growth of Li dendrites.[6] In this work, we leveraged our understanding of the advantageous solvation structures inherent to a fluorinated ester to design a partially ion-paired electrolyte for wide-temperature Li batteries with high energy density, which integrates the advantages of both aforementioned electrolyte systems, overcoming their respective design limitations.

To balance the salt dissociation ability and the desolvation ability, a series of carboxylate esters with different lengths of alkyl chains, and varying degrees of fluorination are selected as the primary solvent. Reduced alkyl chain length in the carboxylate electrolyte weakens its binding with Li^+ ions, facilitating desolvation and improving Li metal CEs as observed (97.4 versus 96.9 % for methyl acetate (MA) and methyl propionate (MP) electrolyte systems, respectively). Methyl 3,3,3-trifluoropionate (MTFP) with partially fluorinated alkyl chains exhibits weaker Li^+ ion solvation ability and superior Li metal compatibility (CEs: 99.3 %). The same trends were found at elevated temperatures (CEs: 99.0, 96.9, and 96.6 % for MTFP, MA, and MP electrolyte systems, respectively). However, only the MTFP electrolyte system with partially fluorinated carboxylate and carbonate esters could maintain high Li metal compatibility at subzero temperatures, which allows Li||SPAN fully cell with high SPAN loading ($>3.5\,mAh\,cm^{-2}$) and thin Li anode (50 μm) to cycle stably at −40, 23, and 50 °C. We attribute this to the temperature-resilient physiochemical property of partially fluorinated carboxylates as the primary solvent and the strong bonding of Li^+/anion and Li^+/fluorinated co-solvent in a moderate ion-pairing solvation structure, which allows a facile desolvation and LiF-dominated interphases without noticeably scarifying the ionic conductivity ($>1\,mS\,cm^{-1}$ even at −40 °C).

Results and Discussion

To provide a viable operation of Li metal batteries (LMBs) at a wide-temperature environment, MP solvents with both low melting (−88 °C) and high boiling (80 °C) points were selected as the primary basis of this investigation. Lithium bis(fluorosulfonyl)imide (LiFSI) and fluoroethylene carbonate (FEC) are employed as the Li salt (1 M) and co-solvent additive (10 % by volume), respectively, both of which are known to stabilize the SEI with abundant LiF species. This system has been well established to provide reversible SPAN performance at ambient conditions.[2c,3c,12a] While the underlying mechanism of poor behavior toward the Li metal side under extreme conditions is still unclear, it is likely attributed to the significantly increased charge-transfer resistance at low temperatures, due to its inherently strong Li^+-solvent binding.[12a]

To examine the solvation effects, a series of derivatives based on the MP solvent was designed by modifying its alkyl chains (Figure 1a). Carboxylate solvents with short alkyl

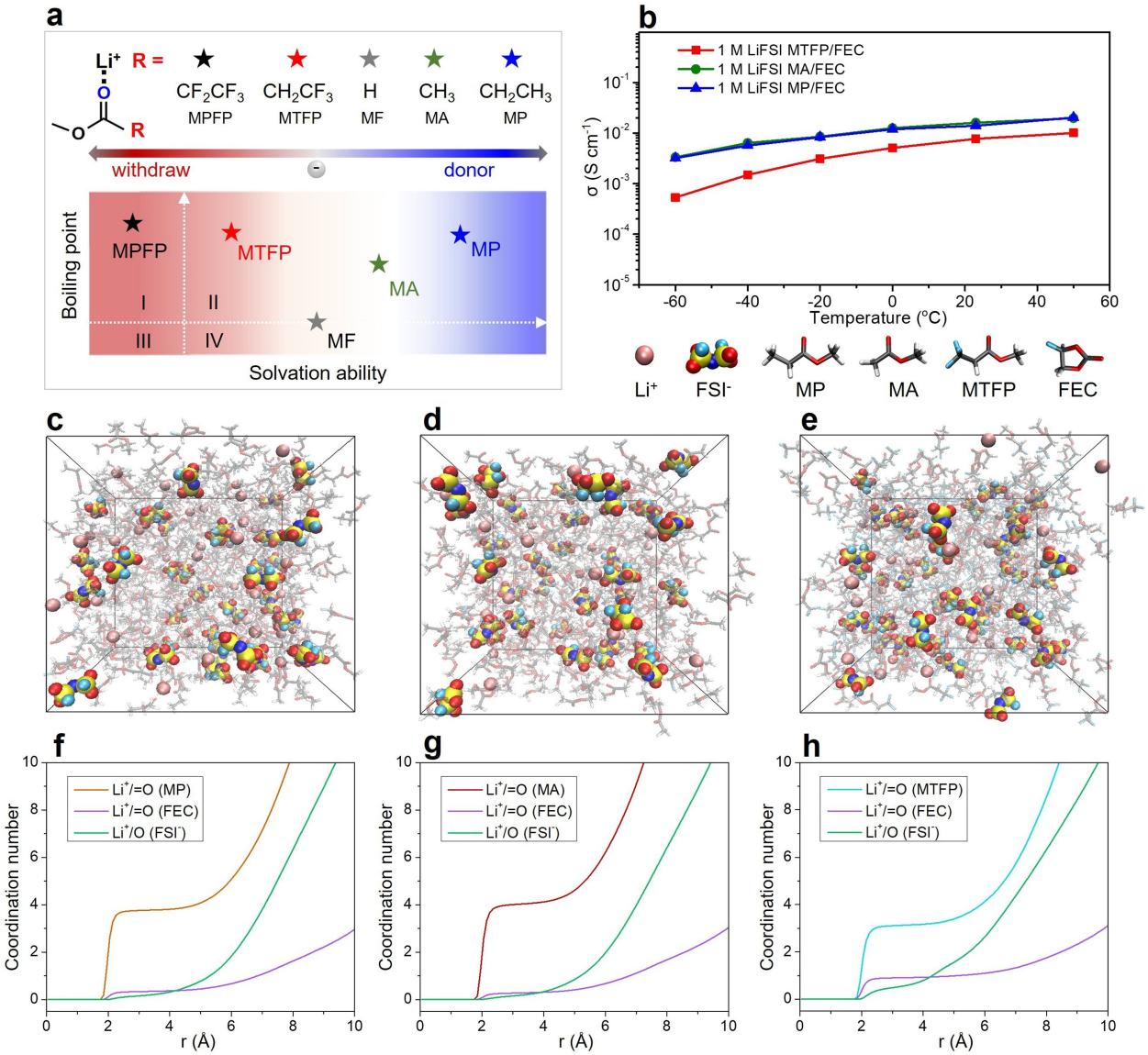

Figure 1. Electrolyte design. (a) Schematic showing the molecular structure modulation of carboxylate derivatives and the boiling point versus solvation ability of various carboxylate derivatives. (b) Ionic conductivity of selected electrolyte systems at different temperatures. (c–e) Snapshots of the simulated cells and (f–h) Li^+ radial distribution functions of selected electrolytes: (c, f) 1 M LiFSI MP/FEC, (d, g) 1 M LiFSI MA/FEC, and (e, h) 1 M LiFSI MTFP/FEC.

chains exhibit lower melting points which are highly desirable for low-temperature systems. In addition, short alkyl chain solvents will have lower polarizability which could be the underlying reason for weak Li^+-solvent binding and consequent facile desolvation, especially at lower temperatures. Nevertheless, reduced-sized carboxylate solvent encounters high volatility and low boiling point, even close to the ambient condition (i.e., methyl formate (MF), b.p.: 32 °C), which is an undesired physical property of the solvent for high-temperature conditions. To balance the melting and boiling points for wide-temperature operations, solvation fluorination can be a wise alternative to adjust the Li^+-solvent binding without noticeably sacrificing the high-temperature property. MTFP with a partially fluorinated alkyl chain sustains the ability to dissolve the LiFSI salt very well while a slightly lower ionic conductivity compared with the MP electrolyte systems. The methyl pentafluoropropionate (MPFE) with a fully fluorinated alkyl chain renders a poor salt disassociation ability and thus dissolves negligible lithium salts (Figure 1a).

To preliminarily evaluate the electrolyte behavior at extreme conditions, physical characterization of the selected electrolytes was first conducted. As shown in Figure S1, it was confirmed that all systems of interest remained in a liquid state down to −40 °C, representative of the low melting point of these carboxylate solvents. In addition, the ionic conductivities of each electrolyte were measured from −60 to 50 °C to provide insight into the effect of temperature on ionic transport (Figure 1b). All systems retain ionic conductivities >1 mS cm^{-1} at −40 °C, which is far superior

compared with most reported systems of ether-based LHCEs for Li-S batteries.[6b,10c]

The solvation structures of each electrolyte were simulated via classical molecular dynamics (MD). As presented in Figures 1c–h and S2, the radial distribution functions of Li^+ in 1 M LiFSI MP/FEC and 1 M LiFSI MA/FEC indicated that the first solvation shell of Li^+ ions are primarily coordinated by solvent molecules (4 MP and 4 MA oxygens per Li^+ ion, respectively), a typical feature of SSIP structures. On the contrary, MTFP with identical LiFSI concentrations was predicted to produce a half SSIP and half CIP structure with a coordination number of 3 MTFP, 1 FEC, and 0.5 FSI oxygens per Li^+ ion.

After dissolving LiFSI salts into selected solvents, the Li^+/FSI^- coordination was characterized via Raman spectroscopy (Figure 2a). The Raman shift of the FSI^- anion (LiFSI salts: 774 cm^{-1}) corresponding to S–N–S bending/vibration downshift to around 728 cm^{-1} upon dissolving in MA and MP solvents. Such noticeable deviation (46 cm^{-1}) can be attributed to the strong solvation ability of MA and MP solvents, which dissociate the Li^+/FSI^- pair and induce a SSIP structure. After dissolving LiFSI salts in the MTFP solvents, the Raman shift of S–N–S bending/vibration is deconvolved in two peaks, where the first one (739 cm^{-1}) presents a smaller downshift while the second one appeared at the same position as those of MA and MP electrolyte systems. This indicates two different chemical conditions (CIP and SSIP) for the Li^+/FSI^- coordination in the MTFP electrolyte systems, which is consistent with the aforementioned MD simulation (Figures 1c–h and S2).

The chemical condition of Li^+ in different electrolyte systems was evaluated by the ^7Li NMR (Figure 2b). Because of the same solvation structures, the downfield shift of 1 M LiFSI MA/FEC compared with 1 M LiFSI MP/FEC indicates a weaker solvation ability of MA than MP. The noticeable upfield shift of the MTFP electrolyte system compared to those with MA and MP can be attributed to the change in solvation structures (CIP versus SSIP), leading to more shielded Li^+ nuclei, might mainly attributed to the

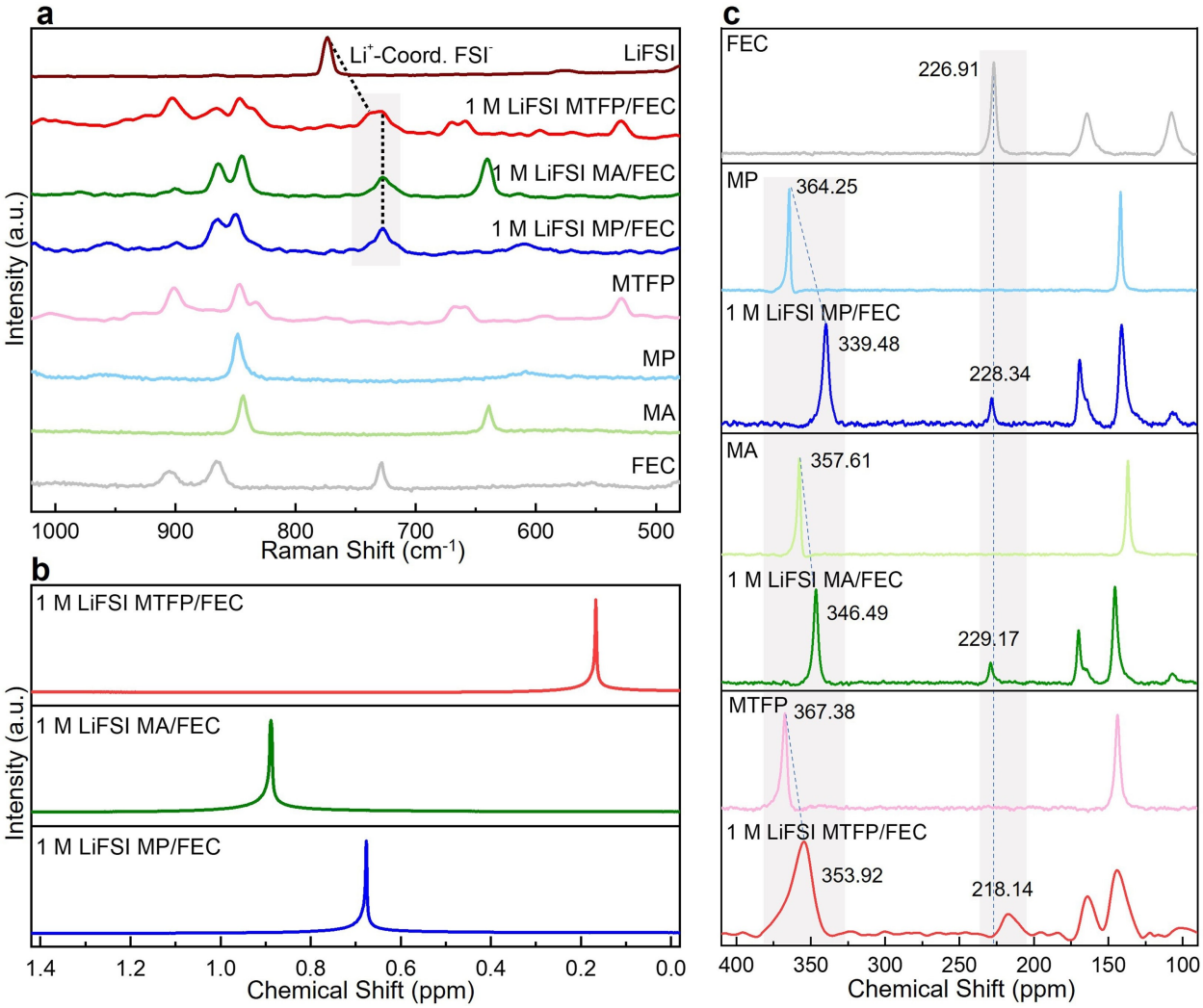

Figure 2. Experimental analysis of formulated electrolytes. (a) Raman, (b) ^7Li nuclear magnetic resonance (NMR), and (c) ^{17}O NMR spectra of selected electrolyte systems.

strong interaction of Li^+ ions toward anion and co-solvent as indicated by the MD simulation (Figures 1e, h, and S2).

To decouple the solvent and anion contribution in the solvation sheath, the chemical condition of oxygen in different electrolyte systems was investigated by the ^{17}O NMR (Figure 2c and S3). The upfield shift of ketonic oxygen in the primary solvent of MA, MP, and MTFP molecules can be attributed to the electron-withdrawing effect of cation. The MP solvent in the 1 M LiFSI MP/FEC presents a larger upfield shift than those of MA and MTFP systems (−24.77 versus −11.12 and −13.46 ppm), indicating a stronger Li^+/carboxylic solvent coordination in the former. On the contrary, the FEC solvent, as a co-solvent in the 1 M LiFSI MTFP/FEC electrolyte system, presents a upfield shift while a downfield shift for those in 1 M LiFSI MP/FEC and 1 M LiFSI MA/FEC electrolyte systems (−8.77 versus 1.43 and 2.26 ppm). Such visible differences indicate the presence of Li^+/FEC coordination in the MTFP system while FEC exists in a free state in the MP and MA electrolyte systems. That is to say, the 1 M LiFSI MTFP/FEC electrolyte presents a low Li^+/main solvent (MTFP) bonding while a strong Li^+/co-solvent (FEC) bonding compared with other two counterparts. Taking the computational simulation and experiment results into account, the weak solvation of partially fluorinated MTFP solvents allows strong coordination of Li^+/anion and Li^+/fluorinated co-solvents, which can be expected to induce the preferential reduction of fluoride-rich species to form LiF-rich SEI as well as facile desolvation kinetics.

To investigate the compatibility of the electrolytes of interest with the Li metal anode, Li||Cu half cells with the aforementioned electrolytes were assembled. The accurate method proposed by Adams et al. was employed to determine the Li plating/stripping CE.[15] Although 1 M LiFSI dissolved in the MA, MP, and MTFP exhibit poor Li metal compatibility (Figure S4), after adding 10 % in vol. of FEC co-solvent, they all present superior Li metal CEs (Figures 3a–c), where the MTFP electrolyte system exhibits a slightly increased CE compared with those of MA and MP electrolyte systems at room temperatures (99.3 versus 97.4 and 96.9 %). They all exhibit good compatibility with Li metal at elevated temperatures (99.0 versus 96.9 and 96.6 %) while only the MTFP system maintains this trend at subzero temperature conditions (97.6 versus 87.9 and 56.7 %).

To emphasize the synergistic effect of the preferential reduction of anions/fluorinated co-solvents for LiF-dominated interphases, the co-solvents in 1 M LiFSI MTFP/FEC electrolyte system are replaced with non-fluorinated counterparts (Figure S5). Upon replacing the FEC with propylene carbonate (PC) and ethylene carbonate (EC),

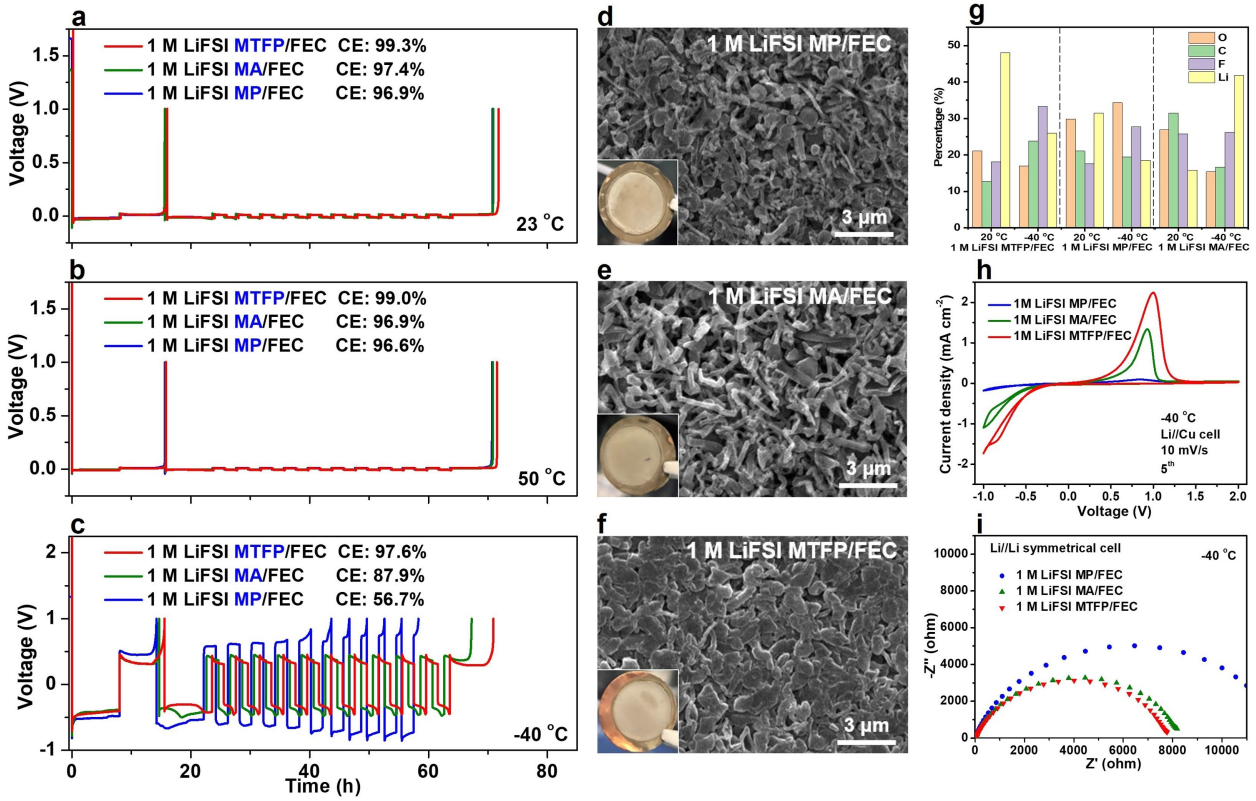

Figure 3. Li metal plating/stripping behaviors. CE-determined curves for the selected electrolytes at (a) 23, (b) 50, (c) −40 °C. Scanning electron microscopy (SEM) images of deposited Li metal in the electrolyte systems of (d) 1 M LiFSI MP/FEC, (e) 1 M LiFSI MA/FEC, and (f) 1 M LiFSI MTFP/FEC. Insets in d-f are the photographs of deposited Li on Cu foil. (g) Element content of O, C, F, and Li of SEI evaluated by the X-ray photoelectron spectroscopy (XPS) testing of plated Li in the selected electrolyte systems. (h) Cyclic voltammetry (CV) curves of Li||Cu cells and (i) Electrochemical impedance spectroscopy (EIS) plots of Li//Li symmetric cells with selected electrolytes at −40 °C.

decreased Li metal CEs of 92.4 % (EC) and 70.6 % (PC) at −40 °C indicates that the selection of fluorinated carbonate co-solvents plays a crucial role in determining the performance of Li metal at low temperatures. To evaluate the salt effect on the LMBs, Li||Cu cells with 1 M $LiPF_6$ MTFP/FEC and 1 M $LiBF_4$ MTFP/FEC were also tested at −40 °C (Figure S6). The worse Li metal CEs of $LiPF_6$ and $LiBF_4$-containing electrolyte systems than those of LiFSI-based electrolyte systems (92.4, 47.4 versus 97.6 %) highlight the advantage of LiFSI as the salts for increased working ability at a wide-temperature condition.

To gain detailed information about the Li metal plating behavior, the Li||Cu cells after plating 4 mAh cm^{-2} Li metal with a current density of 0.5 mA cm^{-2} at 23 and −40 °C were disassembled and their microscopic features of the deposited Li metal on copper foil was examined via SEM. Photographs taken of the Cu electrodes after deposition at 23 °C reveal metallic Li deposits with a silver appearance, which is typically indicative of micron-scale Li deposits (Figure S7). However, a temperature-dependent Li morphology is presented at −40 °C, in which porous and fibrous Li is deposited in MP systems at subzero temperatures while the MA system exhibits a slightly bigger size of Li nanorods (Figures 3d, e). On the contrary, the Li deposited in the MTFP system presents a chunk morphology regardless of the temperature, although it is accompanied by decreased chunk sizes with the drop in temperature (Figure 3f). All the above results highlight the advantageous features of partially ion-paired structures of our all-fluorinated ester-based electrolyte toward Li metal that could sustain under both extreme temperature conditions.

By employing XPS analysis, it was determined that there exist variances in the interfacial chemistry of lithium metal deposited in the MP, MA, and MTFP electrolyte systems (Figures 3g, and S8–S10). Lithium metal cycled in all three electrolyte systems exhibits a comparably high fluorine content (18.1, 25.8, and 17.6 % for MTFP, MA and MP electrolyte systems, respectively). This phenomenon can be ascribed to the preferential reduction of the FEC co-solvents, driven by their high reduction potential. It results in the formation of a LiF-rich SEI. This finding aligns with the nearly identical CEs observed at room temperature (Figure 3a). The significantly higher Li content compared to C, O, and F content within the interphase layer of electrodes cycled with the MTFP electrolytes implies a lower degree of solvent decomposition. This observation reinforces the slightly higher CEs observed in the MTFP electrolyte system. When exposed to subzero temperatures, the MTFP electrolyte systems exhibit a significantly higher fluorine content compared to the MA and MP electrolyte systems (33.3 versus 26.2 and 27.7 %). This divergence substantiates the noticeably high CEs of the MTFP electrolyte system relative to other two counterparts at low temperatures. This can be attributed to the presence of a half cation/anion pair in the 1 M LiFSI MTFP/FEC system. The weak solvation of the partially fluorinated MTFP promotes strong coordination of Li^+/FSI and Li^+/FEC, leading to the formation of LiF-rich SEI derived from both inorganic anions and fluorinated additives. Such a ceramic-rich SEI with high interfacial energy serves to suppress dendrite growth while promoting a planar growth of Li metal especially at reduced temperatures. It is worth noting that all electrolyte systems remain in a liquid state at −40 °C, where the MTFP electrolyte system presents a slightly lower conductivity (Figures 1b and S1). Therefore, the salient deviation of Li metal performance at low temperatures cannot be attributed to the reduction of bulk ion transfer in the electrolytes at reduced temperatures.

To investigate their kinetic behavior at reduced temperatures, we conducted the CV testing of Li||Cu cells at −40 °C (Figure 3h). The onset potential for the MTFP electrolyte system achieved through negative scanning is significantly lower than those of the MP and MA electrolyte systems. This observation suggests a lower overpotential for the nucleation of Li in the MTFP electrolyte system. In addition, the high response current with the increase of testing potential for the MTFP electrolyte system indicates a facile kinetic for Li deposition at subzero temperatures. During the subsequent positive scan of CV (Li stripping stage), a much faster current response and large peak area (higher capacity) in MTFP electrolyte systems than those in MP and MA electrolyte systems signify the fast reaction kinetics and superior Li stripping performances.[16]

To distinguish the underlying drives for the deviation on the Li plating process at reduced temperatures, the diffusion of solvated Li^+ in the bulk electrolyte, Li^+ desolvation at SEI/electrolyte interface, and Li^+ diffusion through SEI is evaluated via temperature-dependent EIS. The EIS of symmetric Li||Li cells was applied in addition to the EIS of SPAN||SPAN symmetric cells to deconvolute the respective impedance contributions (Figures 3i and S11). A noticeably larger impedance of the MP-based electrolyte system than those with MA and MTFP was found, which could be attributed to the strong Li^+/solvent binding as indicated by the results of ^{7}Li and ^{17}O NMR tests (Figure 2). All the above results indicate that MTFP electrolyte system with a partially ion-paired structure allows facile charge transfer and desolvation processes under wide-temperature ranges, which dominate the low-temperature performances. The advantageous features are beneficial for promoting uniform Li deposition and suppressing the Li dendrites even at extreme temperature conditions.

To further examine the potential of the electrolyte system toward practical LMBs at a wide-temperature range, Li||SPAN full cells with a high mass loading of ≈3.5 mAh cm^{-2} SPAN and low negative-to-positive capacity (N/P) ratio of ≈1.7 were assembled and tested at variable temperatures from −40 to 50 °C (Figure 4). The full cells employing 1 M LiFSI MTFP/FEC delivered high energy density of ≈850 Wh/Kg_{SPAN} (stack energy density: ≈200 Wh/kg, Table S1) and cycling stability over 180 cycles at room temperature (Figure 4a). At elevated temperatures, the Li||SPAN cells with 1 M LiFSI MTFP/FEC produced increased energy density of ≈1110 Wh/Kg_{SPAN} and were cycled well around 80 cycles while less than 30 cycles for those with MA and MP electrolyte systems (Figure 4b). Although the Li||SPAN half cells with a low SPAN loading (< 1 mAh cm^{-2}) and thick Li metal (300 μm) could be cycled

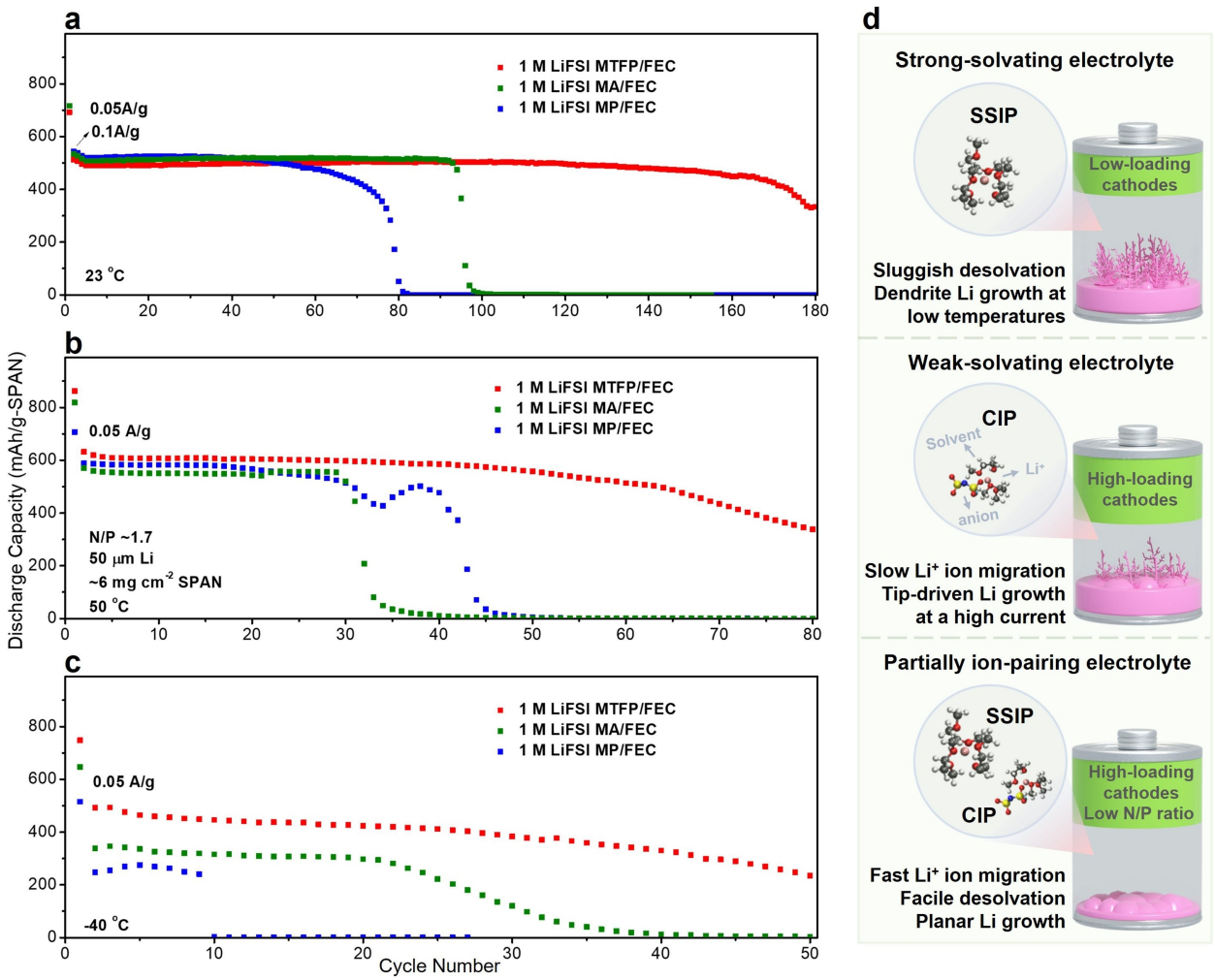

Figure 4. Full cell testing at extreme conditions. (a–c) Cycling performance of Li||SPAN full cells in selected electrolytes at (a) 23, (b) 50, and (c) −40 °C. (d) Schematic showing the Li-S batteries with different solvation electrolytes under extreme operating conditions.

well at −40 °C in our previous work,[12a] the poor Li metal compatibly renders mediocre cycling stability of Li||SPAN full cells with a low N/P ratio and high SPAN loading as shown in Figure 4c. The full cell with MA presents a slightly improved cycling performance, due to slightly higher Li CEs and facile desolvation kinetics (Figure 3). The cells with MTFP electrolyte system present both superior low-temperature cycling stability and energy density compared with those of MA and MP electrolyte systems (≈620 vs 325, 220 Wh/Kg_{SPAN}), attributed to the facile desolvation as well as the strong Li^+/FEC and Li^+/FSI^- bonding in the half cation/anion pair structures to maintain an anion and fluorinated co-solvent-derived LiF-rich SEI at a wide-temperature condition. The above results further suggest the promise of electrolytes with both fluorinated co-solvent and anion involving a half SSIP and a half CIP structure for wide-temperature Li||SPAN batteries with a high areal loading cathode (Figure 4d).

Conclusion

In summary, an all-fluorinated ester-based electrolyte comprising partially fluorinated carboxylate and carbonate esters was developed for high areal loading Li-S full cells operated at extreme temperatures. Both experiments and computational simulations show a strong Li^+/anion and Li^+/fluorinated co-solvent binding in the partially fluorinated carboxylate and carbonate solvent system, compared with those of non-fluorinated counterparts. This all-fluorinated electrolyte with a half cation/anion pair endows a facile desolvation and LiF-dominated interphases without compromising ionic conductivity even at a wide-temperature range. This work establishes new design principles for optimizing future electrochemical devices with tunable salt dissociation and solvent desolvation properties under a wide-temperature range. It also provides a promising path for designing temperature-resilient electrolytes to support high energy-density rechargeable batteries operating in extreme conditions.

Acknowledgements

This research was supported by NASA Space Technology Graduate Research Opportunity 80NSSC20K1174. This work was partially supported by NSF through the UC San Diego Materials Research Science and Engineering Center (UCSD MRSEC), DMR-2011924. This work was performed in part at the San Diego Nanotechnology Infrastructure (SDNI) of UCSD, a member of the National Nanotechnology Coordinated Infrastructure, which is supported by the National Science Foundation (Grant ECCS-1542148). This work also used CPU time at the San Diego Supercomputing Center through allocation DMR190106 from the Advanced Cyberinfrastructure Coordination Ecosystem: Services & Support (ACCESS) program, which is supported by NSF grants #2138259, #2138286, #2138307, #2137603, and #2138296.

Conflict of Interest

The authors declare that they have no competing interests.

Data Availability Statement

All data needed to evaluate the conclusion in the paper are present in the main text and/or the Supporting Information.

Keywords: Battery · Electrolyte · Extreme Temperatures · Ion Solvation · Ion Transports

[1] a) W.-J. Chen, B.-Q. Li, C.-X. Zhao, M. Zhao, T.-Q. Yuan, R.-C. Sun, J.-Q. Huang, Q. Zhang, *Angew. Chem. Int. Ed.* **2020**, *59*, 10732–10745; b) A. Bhargav, J. He, A. Gupta, A. Manthiram, *Joule* **2020**, *4*, 285–291; c) C. Y. Kwok, S. Xu, I. Kochetkov, L. Zhou, L. F. Nazar, *Energy Environ. Sci.* **2023**, *16*, 610–618.

[2] a) Y. Liu, Y. Elias, J. Meng, D. Aurbach, R. Zou, D. Xia, Q. Pang, *Joule* **2021**, *5*, 2323–2364; b) W. Xue, Z. Shi, L. Suo, C. Wang, Z. Wang, H. Wang, K. P. So, A. Maurano, D. Yu, Y. Chen, L. Qie, Z. Zhu, G. Xu, J. Kong, J. Li *Nat. Energy* **2019**, *4*, 374–382; c) Y. Li, S. Guo, *Matter* **2021**, *4*, 1142–1188.

[3] a) J. Wu, S. Liu, F. Han, X. Yao, C. Wang, *Adv. Mater.* **2021**, *33*, 2000751; b) S. Wang, B. Lu, D. Cheng, Z. Wu, S. Feng, M. Zhang, W. Li, Q. Miao, M. Patel, J. Feng, E. Hopkins, J. Zhou, S. Parab, B. Bhamwala, B. Liaw, Y. S. Meng, P. Liu, *J. Am. Chem. Soc.* **2023**, *145*, 9624–9633; c) H. Yang, J. Chen, J. Yang, J. Wang, *Angew. Chem.* **2020**, *132*, 7374–7386.

[4] a) S. Wei, L. Ma, K. E. Hendrickson, Z. Tu, L. A. Archer, *J. Am. Chem. Soc.* **2015**, *137*, 12143–12152; b) Z. Shen, W. Zhang, S. Mao, S. Li, X. Wang, Y. Lu, *ACS Energy Lett.* **2021**, *6*, 2673–2681; c) X. Chen, L. Peng, L. Wang, J. Yang, Z. Hao, J. Xiang, K. Yuan, Y. Huang, B. Shan, L. Yuan, J. Xie, *Nat. Commun.* **2019**, *10*, 1021.

[5] a) H. Kim, J.-Y. Hwang, Y.-G. Ham, H.-N. Choi, M. H. Alfaruqi, J. Kim, C. S. Yoon, Y.-K. Sun, *ACS Nano* **2023**, *17*, 14032–14042; b) Y. Yang, Y. Chen, L. Tan, J. Zhang, N. Li, X. Ji, Y. Zhu, *Angew. Chem. Int. Ed.* **2022**, *61*, e202209619; c) W. Shin, L. Zhu, H. Jiang, W. F. Stickle, C. Fang, C. Liu, J. Lu, X. Ji, *Mater. Today* **2020**, *40*, 63–71; d) Y. Yamada, J. Wang, S. Ko, E. Watanabe, A. Yamada, *Nat. Energy* **2019**, *4*, 269–280.

[6] a) A. C. Thenuwara, P. P. Shetty, M. T. McDowell, *Nano Lett.* **2019**, *19*, 8664–8672; b) J. Holoubek, K. Kim, Y. Yin, Z. Wu, H. Liu, M. Li, A. Chen, H. Gao, G. Cai, T. A. Pascal, P. Liu, Z. Chen, *Energy Environ. Sci.* **2022**, *15*, 1647–1658; c) C. Wang, A. C. Thenuwara, J. Luo, P. P. Shetty, M. T. McDowell, H. Zhu, S. Posada-Pérez, H. Xiong, G. Hautier, W. Li, *Nat. Commun.* **2022**, *13*, 4934; d) G. Cai, Y. Yin, D. Xia, A. A. Chen, J. Holoubek, J. Scharf, Y. Yang, K. H. Koh, M. Li, D. M. Davies, M. Mayer, T. H. Han, Y. S. Meng, T. A. Pascal, Z. Chen, *Nat. Commun.* **2021**, *12*, 3395.

[7] J. Holoubek, H. Liu, Z. Wu, Y. Yin, X. Xing, G. Cai, S. Yu, H. Zhou, T. A. Pascal, Z. Chen, P. Liu, *Nat. Energy* **2021**, *6*, 303–313.

[8] a) G. Cai, A. A. Chen, S. Lin, D. J. Lee, K. Yu, J. Holoubek, Y. Yin, A. U. Mu, Y. S. Meng, P. Liu, S. M. Cohen, T. A. Pascal, Z. Chen, *Nano Lett.* **2023**, *23*, 7062–7069; b) G. Cai, J. Holoubek, M. Li, H. Gao, Y. Yin, S. Yu, H. Liu, T. A. Pascal, P. Liu, Z. Chen, *Proc. Natl. Acad. Sci. USA* **2022**, *119*, e2200392119.

[9] a) Z. Wu, H. Liu, S. Yu, P. Liu, *J. Electrochem. Soc.* **2021**, *168*, 110504; b) Z. Wu, H. Liu, J. Holoubek, C. Anderson, L. Shi, H. Khemchandani, D. Lu, D. Liu, C. Niu, J. Xiao, P. Liu, *ACS Energy Lett.* **2022**, *7*, 2701–2710.

[10] a) Y. Zhao, T. Zhou, M. Mensi, J. W. Choi, A. Coskun, *Nat. Commun.* **2023**, *14*, 299; b) G. Zhang, J. Chang, L. Wang, J. Li, C. Wang, R. Wang, G. Shi, K. Yu, W. Huang, H. Zheng, T. Wu, Y. Deng, J. Lu, *Nat. Commun.* **2023**, *14*, 1081; c) J. Zheng, S. Chen, W. Zhao, J. Song, M. H. Engelhard, J.-G. Zhang, *ACS Energy Lett.* **2018**, *3*, 315–321.

[11] a) W. Zhang, H. Xia, Z. Zhu, Z. Lv, S. Cao, J. Wei, Y. Luo, Y. Xiao, L. Liu, X. Chen, *CCS Chem.* **2021**, *3*, 1245–1255; b) Y. Gao, T. Rojas, K. Wang, S. Liu, D. Wang, T. Chen, H. Wang, A. T. Ngo, D. Wang, *Nat. Energy* **2020**, *5*, 534–542; c) P. Xiao, R. Luo, Z. Piao, C. Li, J. Wang, K. Yu, G. Zhou, H.-M. Cheng, *ACS Energy Lett.* **2021**, *6*, 3170–3179; d) Z. Wang, Z. Sun, Y. Shi, F. Qi, X. Gao, H. Yang, H. M. Cheng, F. Li, *Adv. Energy Mater.* **2021**, *11*, 2100935; e) S. Lin, H. Hua, P. Lai, J. Zhao, *Adv. Energy Mater.* **2021**, *11*, 2101775.

[12] a) G. Cai, J. Holoubek, D. Xia, M. Li, Y. Yin, X. Xing, P. Liu, Z. Chen, *Chem. Commun.* **2020**, *56*, 9114–9117; b) Y. Mo, G. Liu, Y. Yin, M. Tao, J. Chen, Y. Peng, Y. Wang, Y. Yang, C. Wang, X. Dong, Y. Xia, *Adv. Energy Mater.* **2023**, *13*, 2301285; c) X. Dong, Z. Guo, Z. Guo, Y. Wang, Y. Xia, *Joule* **2018**, *2*, 902–913.

[13] A. Gupta, A. Bhargav, A. Manthiram, *Chem. Mater.* **2021**, *33*, 3457–3466.

[14] X. Fan, X. Ji, L. Chen, J. Chen, T. Deng, F. Han, J. Yue, N. Piao, R. Wang, X. Zhou, X. Xiao, L. Chen, C. Wang, *Nat. Energy* **2019**, *4*, 882–890.

[15] B. D. Adams, J. Zheng, X. Ren, W. Xu, J.-G. Zhang, *Adv. Energy Mater.* **2018**, *8*, 1702097.

[16] X. Wang, S. Wang, H. Wang, W. Tu, Y. Zhao, S. Li, Q. Liu, J. Wu, Y. Fu, C. Han, F. Kang, B. Li, *Adv. Mater.* **2021**, *33*, 2007945.

Manuscript received: November 5, 2023
Accepted manuscript online: December 6, 2023
Version of record online: December 22, 2023